Performance Analysis of Four Conceptual Designs for the Air Based Photovoltaic / Thermal Collectors

Karima Esmail Amori **Mustafa Adil Al-Damook**
Assistant Professor
Univ. of Baghdad/ Mech. Eng. Dept. , Aljaderiya - Baghdad-Iraq
drkarimaa@yahoo.com ma_eng80@yahoo.com

ABSTRACT

The thermal and electrical performance of different designs of air based hybrid photovoltaic/thermal collectors is investigated experimentally and theoretically. The circulating air is used to cool PV panels and to collect the absorbed energy to improve their performance. Four different collectors have been designed, manufactured and instrumented namely; double PV panels without cooling (model I), single duct double pass collector (model II), double duct single pass (model III), and single duct single pass (model IV) . Each collector consists of: channel duct, glass cover, axial fan to circulate air and two PV panel in parallel connection. The temperature of the upper and lower surfaces of PV panels, air temperature, air flow rate, air pressure drop, wind speed, solar radiation and ambient temperature were measured. The power produced by solar cells is measured also. A theoretical model has been developed for the collector model IV based on energy balance principle. The prediction of the thermal and hydraulic performance was obtained for the fourth model of PV/T collector by developing a Matlab computer program to solve the numerical model. The experimental results show that the combined efficiency of model III is higher than that of models II and IV. The pressure drop of model III is less than that of models I and IV, by (43.67% and 49%). The average percentage error between the theoretical and experimental results was 9.67%.

Keywords: solar energy; hybrid collector; PV/T; thermal; electrical; performance; air based collector.

تحليل الأداء لتصاميم مختلفة لمجمعات شمسية هوائية حرارية/ فوتوفولطائية

كريمة اسماعيل عموري **مصطفى عادل عبد الرحيم**
أستاذ مساعد
جامعة بغداد- كلية الهندسة – قسم الميكانيك

الخلاصة

تم التحقيق عمليا من الأداء الحراري والكهربائي لتصاميم مختلفة لمجمعات شمسية هوائية مهجنة (فوتوفولتائية/ حرارية). استخدم الهواء لتبريد الألواح الشمسية وتجميع الطاقة الممتصة لتحسين اداء الالواح. تم تصميم وتصنيع وتجهيز اربعة مجمعات شمسية مختلفة بأجهزة القياس ، المجمعات كانت لوحين شمسيين مربوطين بدون تبريد (نموذج I) ، مجمع ذومجرى منفرد ومرور مزدوج للمائع (نموذج II) ، مجريين مع مرور منفرد للمائع(نموذج III) ، و مجرى منفرد ومرور منفرد(نموذج IV). يتكون كل مجمع شمسي من: مجرى، غطاء زجاجي، مروحة محورية لتدوير الهواء ولوحين شمسيين مربوطان على التوازي. قيست درجة حرارة السطح العلوي والسفلي للألواح ، درجة حرارة الهواء، معدل جريان الهواء، وهبوط الضغط له، سرعة الرياح، الأشعاع الشمسي، ودرجة حرارة الجو والقدرة المنتجة من قبل الألواح الشمسية. تم بناء نموذج نظري للمجمع الشمسي الرابع بأعتماد مبدأ الأتزان الحراري. تم التوصل الى تخمين الأداء الحراري والهيدروليكي للنموذج الرابع ببناء برنامج حاسوبي بلغة ماتلاب لحل النموذج الرياضي. بينت النتائج العملية ان الكفاءة المركبة للنموذج الثالث كانت اكبر من تلك الخاصة بالنموذج الثاني والرابع. ان هبوط الضغط للنموذج الثالث كان اقل من ذلك المسجل للنموذج الثاني والرابع بمقدار (43.67% و 49%). أن متوسط نسبة الخطأ المئوية بين النتائج العملية والنظرية كانت 9.67%.

الكلمات الرئيسية: طاقة شمسية، مجمع هجين ، حراري، كهربائي ، اداء ، مجمع هوائي.

1. INTRODUCTION

Photovoltaic thermal hybrid solar collectors (hybrid PV/T systems), are systems that convert solar radiation into thermal and electrical energy. These systems combine a photovoltaic cell, with a solar thermal collector which converts part of the solar radiation (electromagnetic radiation (photons)) into electricity, and the other part is an energy absorbed by the black surface which heats a flowing fluid. Photovoltaic (PV) cells suffer from a drop in efficiency with the rise in their temperature.

Many experimental studies have been reported on the photovoltaic-thermal (PV/T) system, **Kern and Russell 1978.** presented the concept of PV/T collector using water or air as a fluid for removing the absorbed energy. **Raghuraman 1981.** developed two separate one-dimensional models for the prediction of the thermal and electrical performance of both liquid and air flat plate (photovoltaic/ thermal) collectors. **Garg and Adhikari 1997.**analyzed a PV/T air heating system of a single and double glass covers. **Sopian et.al. 2000.** developed and tested a double pass photovoltaic thermal solar collector suitable for solar drying applications. **Chow et al. 2003.** investigated the BIPVT options of a hotel building in South China at (22.2^{o} N). The PV/T face was attached to a full day air conditioned service room to investigate its cooling by means of natural flow of air behind the PV models. **Othman et al. 2005.**studied theoretically and experimentally the PV/T solar air collector with concentrating reflectors. **Shahsavar et al. 2010.** designed, built and tested a PV/T air collector in Kerman, Iran under natural and forced convection with two, four and eight fans operating together to circulate air. **Prashant et al. 2011.**presented a new design of a parallel flow solar air heater with packed material in its upper channel to be capable of providing a higher heat flux compared to the conventional non-porous bed double flow systems. The collector efficiency of upward-type double-pass flat plate solar air heaters with fins attached and external recycle is investigated theoretically by **Chii et al. 2011,** and , **Ma et al. 2011**. They proposed a design of a solar collector that is able to provide both hot water and hot air to increase the annual thermal conversion ratio of solar energy.

The objective of the present work is to identify experimentally the electrical and thermal performance of PV/T collectors under Iraq climate conditions considering the effect of air flow rate.

2. EXPERIMENTAL WORK

Four different models of hybrid PV/T collectors are designed manufactured and instrumented. These models are shown in **Figs. 1, 2 and 3**. In these models two PV modules in parallel connection are mounted in wooden structure. The air duct was perfectly sealed to avoid air leakage. Air has been passed through the duct by using a single DC fan of (6 W) power at the duct outlet. The PV/T system has been mounted on a steel frame with the feasibility to change the inclination angle. The specifications for PV module and PV/T collector used in this work are given in Tables 1 and 2 respectively. In model II, air flows in a single duct for one pass over and under the absorber as shown in **Fig.1a**. In model III air flows in two ducts over and under the PV module in the same direction with single pass, while in model IV air passes in a single duct below the absorber only, as shown in **Fig. 3**.

Twenty two calibrated thermocouples of type k are used to measure the temperatures in this work. Ten of them are distributed at equal distances at back surface of the panels with three thermocouples are fixed on the upper surface along the PV panel at distances of (0.1m , 0.3m , 2.2m) from the inlet. Eight thermocouples are distributed along the air duct of models II, III, and IV including the inlet and outlet air temperature, and one thermocouple is fixed on the collector glass cover, as shown in **Fig.4**. The ambient temperature was measured at 1.5m above ground. All thermocouples are connected to a selector switch type K. The air velocity was measured using a multifunctional anemometer device (model (EM-9000). The air pressure drop is measured using

inclined differential manometer between two points namely ducts' inlet and outlet as shown in **Fig.1a**. The pressure drop is calculated from manometers reading (H) as

$$\Delta p = \gamma H.\sin\theta \quad (1)$$

where θ is manometer inclination angle.

The solar radiation is measured by using south facing Solar meter (TES-1333R Data logging) at the same collector tilt angle.

The power generated by the PV panels was calculated according to the equation:

$$P_{pv} = V * I \quad (2)$$

where V is the voltage and I is the current produced by PV panels. These parameters are measured by multimeter model (3500/3600) made in England especially for AC or DC applications.

2.1 Experimental Procedure

The test of the PV/T collectors and PV array for eight months from December 2010 to July 2011 includes.

1. Testing model I without load for ten clear days and with different flow rate ranging from [36.2-83.1] l/s. This test was carried out during December, 2010 and January, 2011.
2. The data of model I & model II were taken at the same time for ten clear days with different flow rate ranging from [66.62-126.5] l/s during February & March, 2011.
3. Model III is tested at flow rate [66.62-126.5] l/s with the same manner in 1 and 2 above during April & May 2011.
4. Model IV is tested during July 2011.

3. THEORETICAL MODEL

The fourth model used in this work is composed of a single glass cover, a PV modules and a well insolated back plate as shown in **Fig.5**. The energy balance principle is applied on each element with the following assumptions: The system is in a quasi-steady state condition, There is no air leakage from the hydraulically smooth flow channel, Heat capacity of the glass cover, enclosed air, PV modules absorber and bottom plates are negligible at steady state, The temperatures of the PV modules, glass, absorber and bottom plates vary only along the x-direction of the air flow, and heat loss from the sides of the duct is very small and hence neglected **, Duffie, and Beckman 1990**. **Fig.5** shows the various heat transfer coefficient along the surface of the system.

- Absorber PV/T (**Fig. 6**)

$$SL_2dx = U_tL_2dx(T_{pm} - T_a) + h_fL_2dx(T_{pm} - T_f) + h_{rpb}L_2dx(T_{pm} - T_{bm}) \quad (3)$$

- Bottom Plate (**Fig**. 7) **(Al-Damook 2011)**

$$h_{rpb}(T_{pm} - T_{bm})L_2dx = h_f(T_{bm} - T_f)L_2dx + U_b(T_{bm} - T_a)L_2dx \quad (4)$$

3.1 Calculation of Heat Transfer Coefficients

3.1.1 Heat Loss Coefficients

The overall heat loss factor consists of top, bottom, and edge heat loss coefficients.

The bottom loss coefficient (Ub) is evaluated by considering conduction and convection losses from the absorber PV/T in the downward direction through the bottom of the collector. It can be evaluated as: **(Sumeet 2010)**

$$U_b = \left[\frac{L_c}{K_c} + \frac{L_w}{K_w} + \frac{1}{h_w}\right]^{-1} \quad (5)$$

where $\mathbf{h_w}$ is the wind heat transfer coefficient, which is calculated from: McAdams model **, Francis 2002**.

$$h_w=5.7+3.8\ V_{wind} \quad (6)$$

The top heat loss U_t is given by: **, Duffie, and Beckman 1990.**

$$\mathbf{U_t}=\left[\frac{1}{\mathbf{h_w}+\mathbf{h_{rw}}}+\frac{1}{\mathbf{h_{pc}}+\mathbf{h_{rpc}}}\right]^{-1} \quad (7)$$

where,

$\mathbf{h_{rw}}$ = radiation heat transfer coefficient between cover glass and the sky given as:

$$h_{rw}=\varepsilon_g\sigma\left(T_c^2+T_s^2\right)(T_c+T_s) \quad (8)$$

$\boldsymbol{\varepsilon_g}$ = glass emittance

σ = Stefan-Boltzmanns' constant equals to $5.67*10^{-8}$ W/m^2.K^4

$\mathbf{T_s}$ = sky temperature is usually calculated from:

$$T_S = 0.0552\ T_{amb}^{1.5} \quad (9)$$

$\mathbf{h_{rpc}}$ = radiant heat transfer coefficient from absorber PV/T to cover is given as:

$$\mathbf{h_{rpc}}=\frac{\boldsymbol{\sigma}(\mathbf{T_{pm}^2}+\mathbf{T_c^2})(\mathbf{T_{pm}}+\mathbf{T_c})}{\frac{1}{\boldsymbol{\varepsilon_p}}+\frac{1}{\boldsymbol{\varepsilon_g}}-1} \quad (10)$$

where $\boldsymbol{\varepsilon_p}$, $\boldsymbol{\varepsilon_g}$ = plate and glass emittance.

3.1.2 Heat Transfer Coefficient in the Upper Channel

The natural convection heat transfer coefficient ($\mathbf{h_{pc}}$) between the absorber plate and glass cover of the collector model IV is estimated by the equation proposed by **Meyer et al. (Hussam 2011)** as:

$$Nu_S = c(Gr)^n \quad (11)$$

where, c and n are constants affected by the tilt angle. These constants are listed in table (3).
The Grashof No. (Gr) is defined as

$$\mathbf{Gr}=\frac{\mathbf{g}\boldsymbol{\beta_v}(\mathbf{T_p}-\mathbf{T_a})\mathbf{L_m^3}}{\boldsymbol{\nu}^2} \quad (12)$$

where: g=Gravitational acceleration (m/s^2). β_v=volumetric expansion coefficient (K-1) given as:

$$\boldsymbol{\beta_v}=\frac{1}{\mathbf{T}} \quad (13)$$

$\mathbf{L_m}$ = Mean space between absorber plate and glass cover (m).

$\boldsymbol{\nu}$ = Kinematic air viscosity (m^2/s).

The convective heat transfer coefficient is then calculated as:

$$\mathbf{h_{pc}} = \frac{\mathbf{NuK_a}}{\mathbf{L_m}} \quad (14)$$

where $\mathbf{K_a}$ is air thermal conductivity (W/m.K)

3.1.3 Heat Transfer Coefficient in Lower Channel

The forced convection heat transfer coefficient between air stream and absorber plate (h_f) of collector model IV and the properties of air are calculated at local fluid temperature (T_f) by: ,**Duffie, and Beckman1990.**

$$Nu_f = 0.0158Re \times P_r^{0.4} \quad (15)$$

where:

$$Re = \frac{\rho V D_h}{\mu} = \frac{2\dot{m}}{(L_2+h)\mu} \quad (16)$$

$\mathbf{D_h}$ = The hydraulic diameter of the air passage is calculated as:

$$\mathbf{D_h} = \frac{2\mathbf{L_2 h}}{\mathbf{L_2 + h}} \quad (17)$$

where $\mathbf{L_2}$ = collector width, h is duct inlet height, $\dot{\mathbf{m}}$ = air flow rate (kg/s.).

μ = air dynamic viscosity (kg/m.s)

Thus, the convective heat transfer coefficient can be obtained as:

$$h_f = \frac{K_a}{D_h} Nu_f \quad (18)$$

A Matlab computer program is developed to solve the numerical model. **Fig 8.** illustrates the flow chart of this program.

4. RESULTS AND DISCUSSION

Fig.(**9** shows the ambient conditions in Fallujah city for selected clear days during the test period namely; (28/12/2010, 28/4/2011 and 2/7/2011. The ambient temperature follows the incident solar radiation from sunrise to solar noon, after which a considerable deviation in its behavior is indicated in April and July.

Fig.**10** demonstrates the effect of PV panel temperature on electrical power generated at different flow rates for models (I , II and III) . It is obvious that the electrical power increases when the panel temperature decreases.

Fig.**11** presents the hourly distribution of combined efficiency, thermal efficiency and electrical efficiency for models I, II and III. Table (4) illustrates a comparison between the electrical and combined efficiencies of models II, and III with model I higher efficiency was recorded for model III.

Fig.**12** shows the effect of air flow rate on average PV panel temperature. The heat transfer coefficient increases with increasing of mass flow rate which leads to absorb more heat and decrease the temperature difference between the surface panel and flowing air. This result agrees with that obtained by **(Jin et al. 2010)**.

Fig. **13** demonstrates the effect of Reynolds number on pressure drop for models II & III. It is clear that the pressure drop increases with increasing of Reynolds number according to:

$$\text{pressure loss} = f_f\left(\frac{L\mu^2}{D_h^5}\rho\right)Re^2 \quad (19)$$

Fig. **14a** shows a comparison between the electrical power produced by models I and II on 29/3/2011. Lower values are indicated for model I than that for model II due to: optical losses, edge losses, difficulty of cleaning the panel, which leads to dust accumulation on the panels.

Fig.**14b** demonstrates hourly temperature distribution of the upper and lower PV panel surfaces on (29/3/2011) for models I & II. The maximum temperature differences between model I and II for the upper and lower surfaces were 14.94 ^oC and 15.2^oC, respectively and the minimum temperature differences were 2.11^oC and 6.7^oC, respectively.

4.1 Comparison with Previous Published Results

A quantitative comparison between the present results and previously reported results is difficult due to the differences in local ambient conditions such as; solar radiation, ambient temperature, wind speed, humidity and the type of the solar panel used. So a qualitative comparison have been adopted as shown in **Fig**.**15**, which illustrates a very good agreement between the present work and the previously published results.

4.2 Comparison between Theoretical and Experimental Values for Model IV

Fig.**16** presents good agreement between theoretical and experimental results of air temperature in the lower channel for model IV. The maximum percentage deviation is 3.41%.

Fig.**17** demonstrates a comparison between theoretical and experimental values of heat gain for model IV. The deviation between them is due to the optical losses because of dust accumulation. The percentage error was 13.2%.

Fig.18 illustrates a comparison between theoretical and experimental values for thermal efficiency. The deviation between them is due to several factor namely:

- Fluctuated wind speed values.
- Over all heat transfer coefficient.
- Variation in real ambient temperature.
- Optical losses.

The maximum percentage deviation was 7.6%.

4.3 Comparison between the Four Models for Multi Parameters

The maximum average parameter values for all measured days (thermal efficiency, electrical efficiency, pressure drop, power consumed (p_c) due to air mass flow rate, power of fan, temperature rise and Reynolds number are given in Table (5) . This table also demonstrates the percentage enhancement for any parameter which is calculated as:

$$\text{Enhancement ratio} = \frac{\text{Max. prarmeter} - \text{Min. prarmeter}}{\text{Min. parameter}} \quad (20)$$

5. CONCLUSIONS

From the experimental investigation of the models I, II, III and IV in Iraq climate conditions, the following conclusions can be concluded. The electric efficiency was a function of PV panel temperature; the increase of temperature above the design temperature decreases the efficiency of the panel. It is found that the acceptable range of temperature and solar radiation were (22^oC-38^oC) and (550 – 850) W/m^2 respectively, and depending on the grade of PV panel used (A, B, C). The thermal efficiency of model III was 102.7 % greater than that of model IV. The thermal efficiency of model III is 26.9 % greater than that of model I. The combined efficiency of model III was 90.4 % greater than that of model IV. The combined efficiency of model III is 5.91 times the efficiency of model I. The total efficiency (combined efficiency) of model III was 9.45 times that of model II in the measured days. The combined efficiency of model (I) is 7.29 times greater than that of model

II in the measured days. The pressure drop inside the duct of model III was 43.67 % less than that of model I in the measured during days despite the fact that mass flow rate for model III was greater than that of model I. The thermal behavior was improved by increasing the flow rate above 130 L/s when the range of solar radiation was above 530 W/m^2. The average percentage error between theoretical and experimental results was 9.67%.

REFERENCES

- Alghareeb, A. A.,1992, *The effect of thermal radiation and heat transfer area on the performance of a solar air heater*, M.Sc. thesis, univ. of Basrah, Chemical Engineering.

- ASHRAE Applications Handbook, 1999. *Chapter 32 by American Society of Heating, Solar Energy Use* (ASHRAE). Atlanta, GA.

- Baa, Y. and Adam, N. 2008, *Performance analysis for flat plate collector with and without porous media*, Journal of Energy in Southern Africa, V.19, No 4.

- Chii, D. H., HoMing, Y., Tsung, C. C., 2011, *Collector efficiency of upward-type double pass solar air heaters with fins attached*, International Communications in Heat and Mass Transfer, V.38, pp. 49–56.

- Chow, T. T., Hand, J. W., Strachan, P. A., 2003, *Building-integrated photovoltaic and thermal applications in a subtropical hotel building, Applied Thermal Engineering*, V.23(16),pp.2035-2049.

- Duffie, J.A., Beckman, W. A., 1990, *Solar Engineering of Thermal Processes , John Wiley & Sons, Inc.*

- Francis, W., 2002, *Heat transfer loss or gain*) coefficients from bare flat plate solar heat collectors, The Zomeworks Program Office of the Double Play System: Summer Cooling and Winter Heating.

- Garg, H. P., Adhikari, R. S., 1997, *Conventional hybrid Photovoltaic/Thermal* (PV/T) air heating collectors: steady-state simulation, Renewable Energy, V.11, No.3, PP.363-385.

- Hussam, H. J., 2011, *Evaluation of a solar assisted desiccant cooling system for a small meeting hall*, M.Sc thesis, university of Baghdad in Mechanical Engineering.

- Jin, L.G., Ibrahim, A., Chean, Y.K., Daghigh, R., Ruslan, H., Mat, S., Othman, M.Y., Sopian, K., 2010, *Evaluation of Single-Pass Photovoltaic-Thermal Air Collector with Rectangle Tunnel Absorber*, American Journal of Applied Sciences, V.7 (2), pp.277-282.

- Kern Jr. EC, Russell Mc., 1978, *Combined Photovoltaic and Thermal Hybrid Collector System*, Proceedings of 13th IEEE Photovoltaic Specialist pp.1153–7.

- Ma J., Sun, W., Ji J., Zhang, Y., Zhang, A., Fan, W., 2011, *Experimental and theoretical study of the efficiency of a dual-function solar collector*, App. Thermal Eng., V.31, pp.1751– 1756.

- Mustafa Adil AlDamook, 2011, *Performance analysis of various conceptual design for the air based Photovoltaic*/Thermal collectors, M.Sc. thesis, Univ. of Baghdad, Dept. of Mech. Eng.

- Otham, M. H., Yatim, B., Sopian, K., AbuBakar, M. N., 2005, *Performance analysis of a double-pass photovoltaic/thermal* (PV/T) solar Collector with CPC and Fins, Renewable Energy V.30,pp .2005-2017.

- Othman YM, Yatim B, Sopian K, AbuBakar M.N., 2007, *Performance studies on a finned double-pass photovoltaic-thermal* (PV/T) solar collector, Desalination V209, pp.43-49.

- Prashant, D., Thakur, N. S., Kumar, A., Singh,S., 2011, *An analytical model to predict the thermal performance of a novel parallel flow packed bed solar air heater*, Applied Energy,V.88 , pp. 2157-2167.

- Raghuraman, P., 1981, *Analytical predictions of liquid and air photovoltaic/Thermal flat plate collect performance*, J. of solar energy eng., V. 103, Nov., PP. 291-298.

- Shahsavar, A., Ameri, M., 2010, *Experimental investigation and modeling of a direct coupled PV/T air collector*, Solar Energy, V.84, pp.1938-1958.

- Sopian, K., Liu, H. T., Kakac, S., Veziroglu, T. N., 2000, *Performance of a double pass photovoltaic thermal solar collector suitable for solar drying systems*, Energy Conversion and Management, V.41, pp.353-365.

- Sopian K., Alghoul M. A., Alfegi E. M., Sulaiman M. Y. and Musa E A., 2009, *Evaluation of thermal efficiency of double-pass solar collector with porous–non porous media*, Renewable Energy, V.34, pp.640–645.

- Sumeet, S., 2010, *Mathematical modeling of solar air heater with different geometries*, M.Sc. thesis, Thapar University, Patiala Mechanical Eng. Dept.

NOMENCLATURE

Latin Symbols		Re	Reynolds No.
A_c	area of PV cell m^2	S	Solar radiation (W/m^2)
A_p	area of absorber plate m^2	S_g	energy absorbed by the glass cover (W/m^2)
Cp	air specific heat (J/kg.K)	S_p	energy absorbed by the absorber plate (W/m^2)
CFD	Computational fluid dynamics	t_c	thickness of PV cells (m)
D	depth of air duct (m)	t_g	thickness of glass cover (m)
D_h	hydraulic diameter of the air duct (m)	t_{in}	thickness of insulation (m)
dx	length of Elemental duct division (m)	T_a	Ambient air temperature (K).
e	root mean square of percentage deviation	T_{bm}	bottom plate temperature (K)
F	Packing factor	T_f	fluid (air) temperature (K)
g	gravitational acceleration (m/s^2)	T_g	Collector glass cover temperature (K).
G	incident solar radiation (W/m^2)	T_{pm}	absorber (PV module) temperature (K).
H	manometer reading (m)	T_{ref}	reference temperature (K).
h_f	fluid convection heat transfer coefficient (W/m^2K)	T_s	sky temperature (K).

h_p	forced convection heat transfer coefficient (W/m^2K)	V_{pv}	PV voltage (volt)
h_{p-g}	free heat transfer coefficient in the air gap (W/m^2)	V_w	wind velocity (m/s)
$h_{r,g-sky}$	radiation heat transfer coefficient between absorber PV/T and sky (W/m^2K)	W	width of the air duct (m)
$h_{r,pb}$	radiation heat transfer coefficient between absorber PV/T and bottom plate (W/m^2K)	U_t	Overall top heat loss coefficient (W/m2.K)
$h_{r,pg}$	radiation heat transfer coefficient between absorber PV/T and glass cover (W/m^2K)	V	PV voltage (Volt)
h_w	wind heat transfer coefficient ($W/m^2.K$),	x	distance along the duct
I	PV current (Amp.)		**Greek Symbols**
K_c	thermal conductivity of bottom plate (W/m.K)	α_c	absorptivity of cells
K_{in}	thermal conductivity of insulation (m)		
K_w	thermal conductivity of wood (m)	α_p	absorptivity of the plate
L	length of absorber plate (m)	β	collector tilt angle (deg)
L_1	Collector Length (m)	ε_g	glass emittance
L_2	Collector width (m)	ε_p	Plate emittance
L_c	thickness of bottom plate (m)	η_c	conversion efficiency of PV module
L_w	thickness of wood (m)	μ	dynamic viscosity (kg/m.s)
$\dot{m}$	air mass flow rate, (kg/s)	ρ	density of manometer fluid (kg/m^3)
Δp	pressure drop (Pa)	σ	Stephen-Boltzmann constant
P_{pv}	power produced by PV (W)	θ	manometer tilt angle (deg)
r	linear coefficient of correlation	τ_g	transmissivity of glass
Ra	air gap Rayleigh No.	τ_{po}	transmissivity of pottant

Table 1. Specification of PV/T collectors.

Collector tilt angle (degree)	44^{o}(II), 23^{o} (III), 5^{o} (VI) **(ASHRAE Handbook 1999)**
Collector length (mm)	3310
Collector width (mm)	580
Overall height (mm)	60
Upper duct height (mm)	35
Lower duct height (mm)	24
Inlet area(mm^2)	70×540 model II 10.2×540 model III
outlet area(mm^2)	70×540 model II, model III
Plate type	Flat plate
Cover material	Ordinary clear glass, $\tau = 0.86$ [Sopain et al. (2009)]
Number of covers	1
Thermal conductivity of Insulation material (Wood panel)	k= 0.059 **(Hussam 2011)**
Back insulation thickness (mm)	20

Table 2. Specification of PV panel.

ELECTRICAL DATA	
Maximum Power at STC	60 W
Maximum Power voltage at STC	17.6 V
Maximum Power Current at STC	3.4 Amp
Open Circuit Voltage (V_{oc})	21.6
Short Circuit Current (I_{sc})	3.74
Operating Temperature	25(^{o}C)
Operating Radiation	1000W/m^2
MECHANICAL DATA	
Cell Type	Poly-crystalline
No. of cells and cells Arrangement	60 (6 x 10)
Dimensions(mm)	1200 x 540 x 32mm
Weight	20kg (44.1 lbs)
Front Cover	Tempered glass
Frame Material	Anodized Aluminum Alloy
Standard Packaging (Modules per Pallet)	20 pcs

Table 3. Constants for Eq.(10).

Tilt angle	c	n
0	0.060	0.410
10	0.065	0.400
20	0.070	0.390
30	0.075	0.380
40	0.080	0.367

Table (4): Comparison between PV/T collectors.
(Values are taken at solar noon)

Compare between Models	Combined Efficiency%	Electrical Efficiency	Ratio B/A
I and II	A=9.55 (model I)	9.55 (model I)	7.2
	B=44 (model II)	9.3 (model II)	
III and II	A= 44 (model II)	9.3 (model II)	1.32
	B= 58 (model III)	6 (model III)	

Table (5): Comparison between daily performance parameters for models II, III, IV.

Parameter	Model II	Model III	Model IV	Enhancement ratio% for (model)
Combined efficiency	65.4	78.7	41.35	90.4%(III)
Thermal efficiency	57.1	72.5	35.8	102.7%(III)
$\Delta p(N/m^2)$	73.5	41.4	77.44	49%(III)
Pc(mW)	67	57.8	95.75	39.7%(III)
Temp. rise(^oC)	7.2	6.23	8.1	30%(IV)
Power fan(W)	33	47	47	21.2(I)

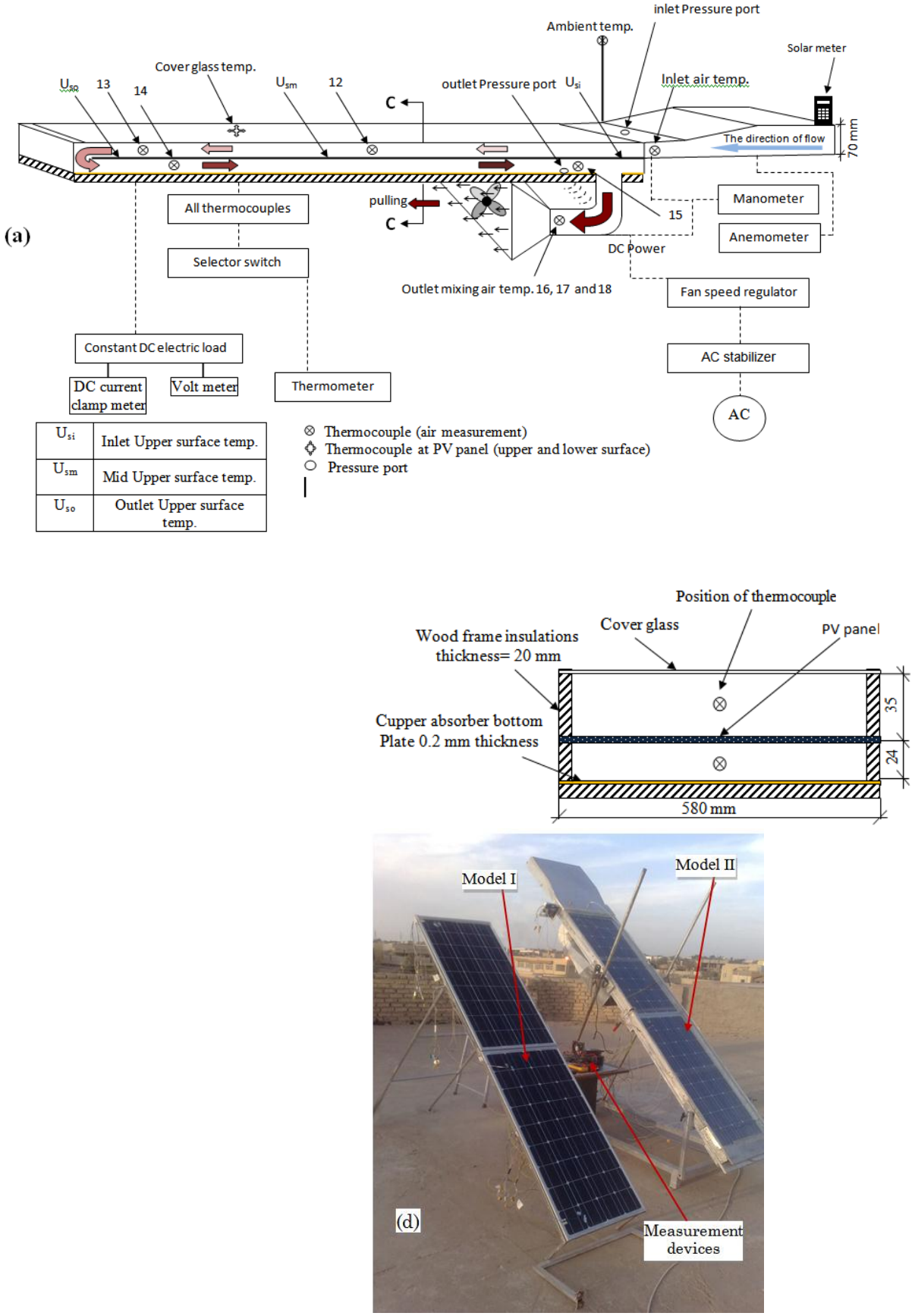

Figure 1. (a) Schematic diagram of experimental setup for model II; (b) Top view of PV panels; (b) Cross section view of C-C, (d) Outdoor test of model I and model II

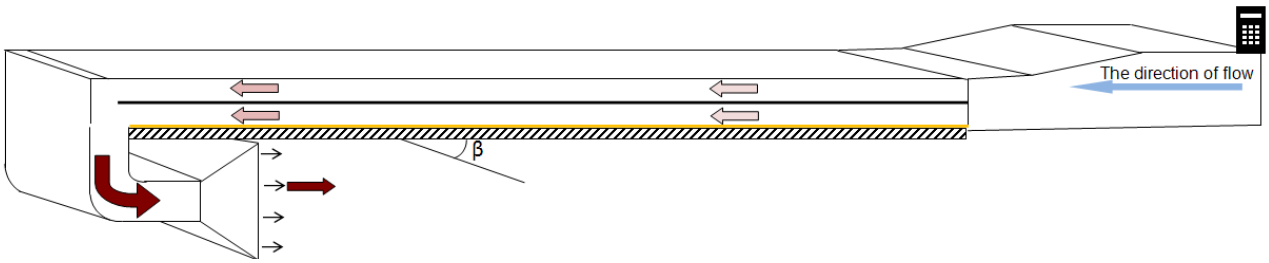

Figure 2. Schematic Diagram of Experimental Setup for Model III.

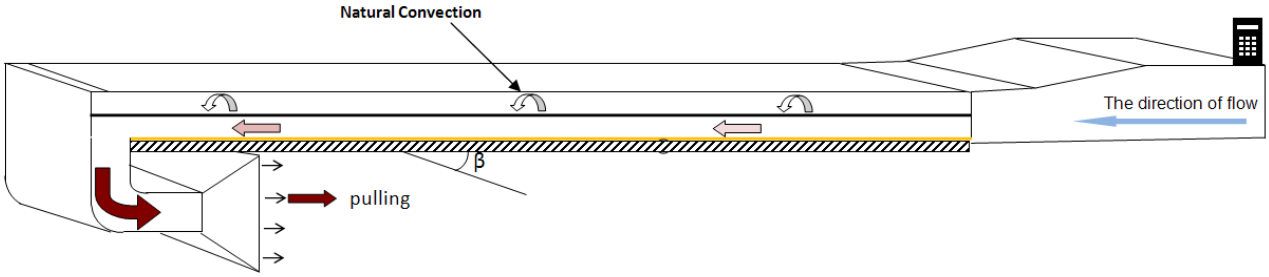

Figure 3. Schematic Diagram of Experimental Setup for Model IV

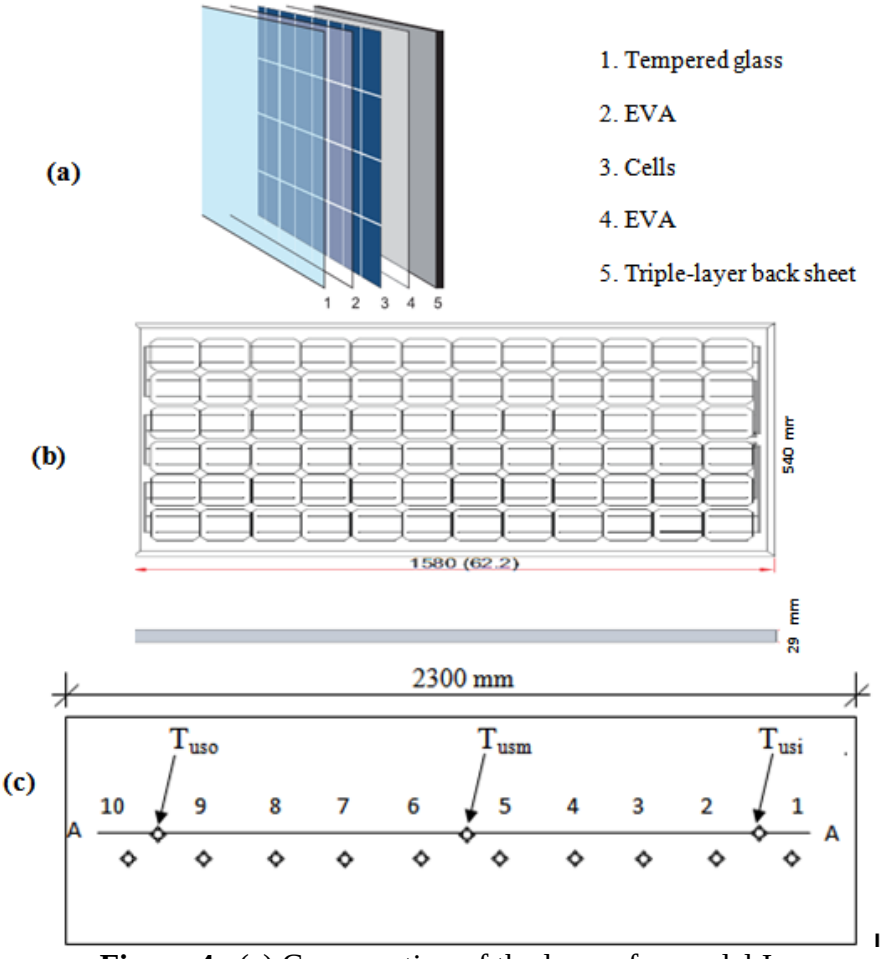

Figure 4. (a) Cross section of the layers for model I,
(b) Top view of PV panel, (c) Thermocouples positions.

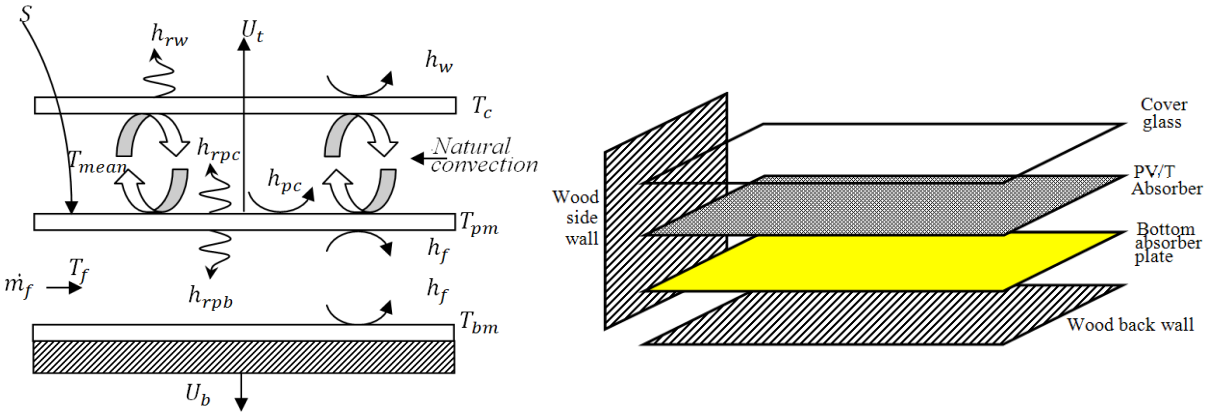

(a) (b)

Figure 5. (a) Various Heat transfer coefficient along the surface of the system. (b)schematic diagram of the studied PV/T air system (Model IV).

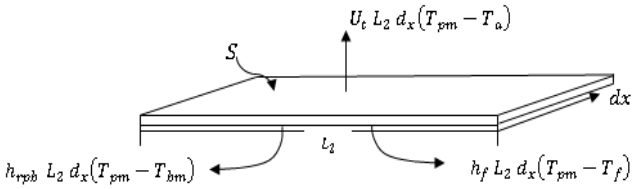

Figure 6. Energy equations for absorber PV/T for model iv

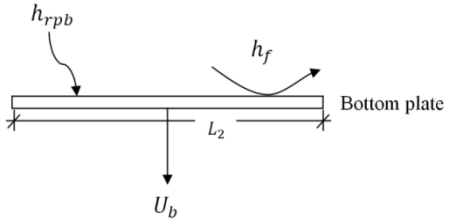

Figure 7. Energy equations for absorber bottom plate for model IV

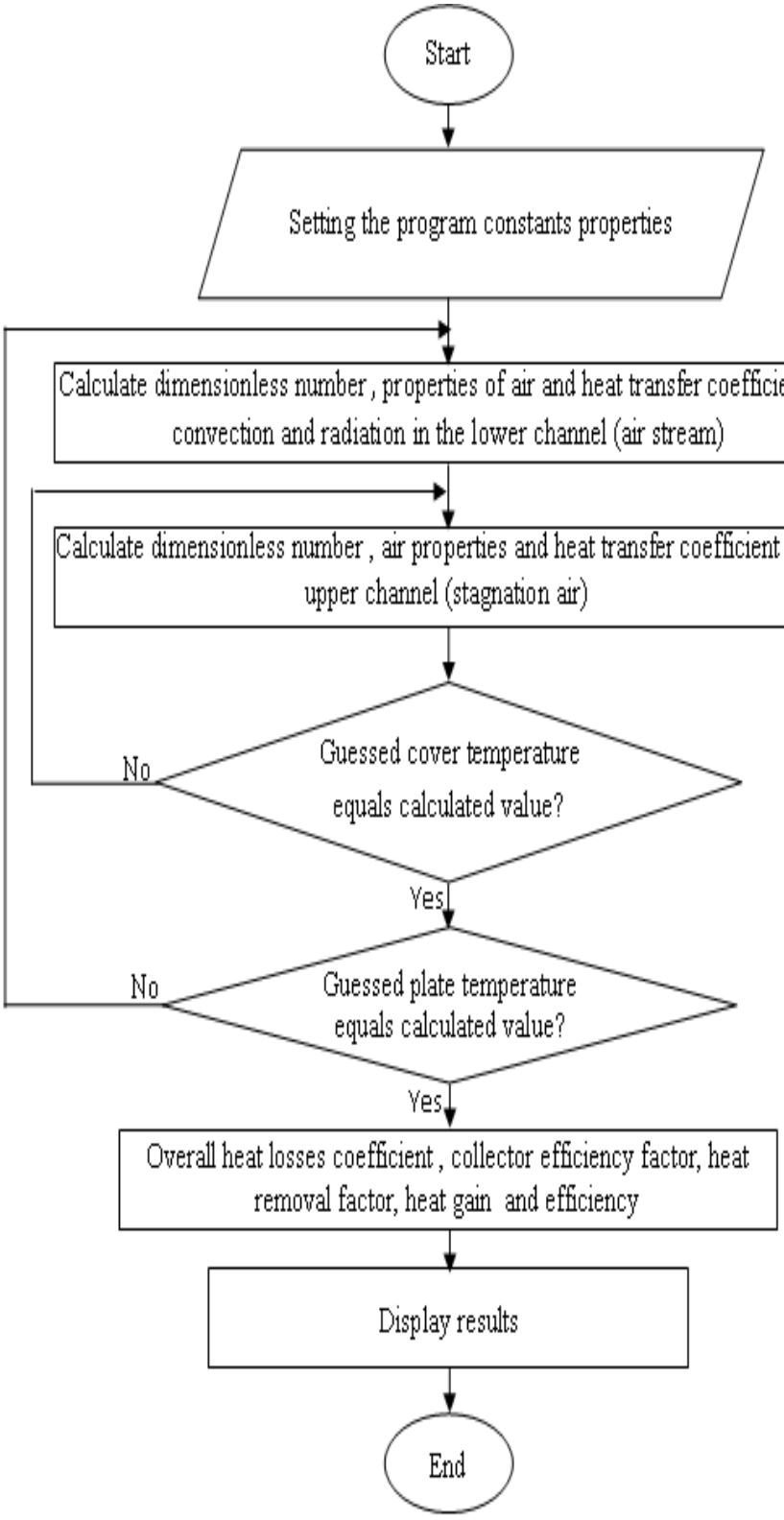

Figure 8. Flow chart of the computer program

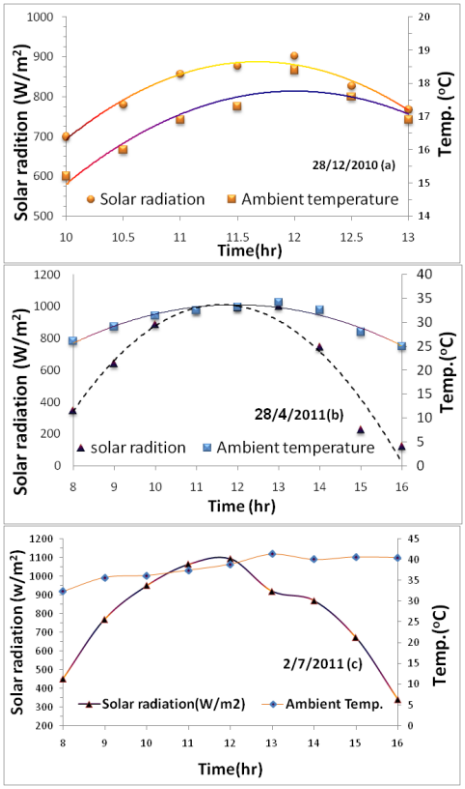

Figure 9. Hourly variation of solar radiation and ambient temperature for selected days from December 2010 to July 2011

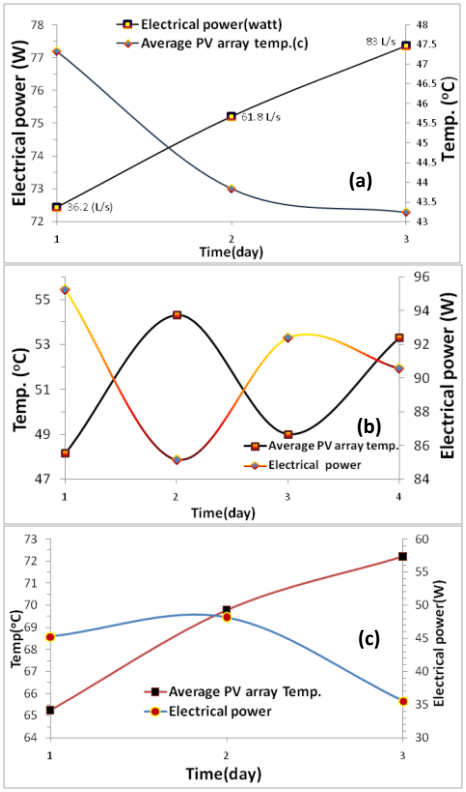

Figure 10. Effect of PV panel temp. on electric power for three models (a) model II (b) model III (c) model IV

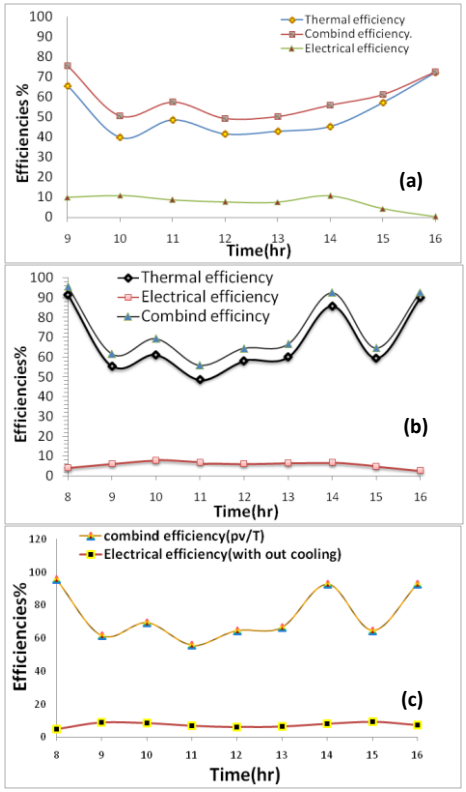

Figure 11. Hourly total efficiency, thermal efficiency and electrical efficiency for a) model II, b) model III, c) models I and III

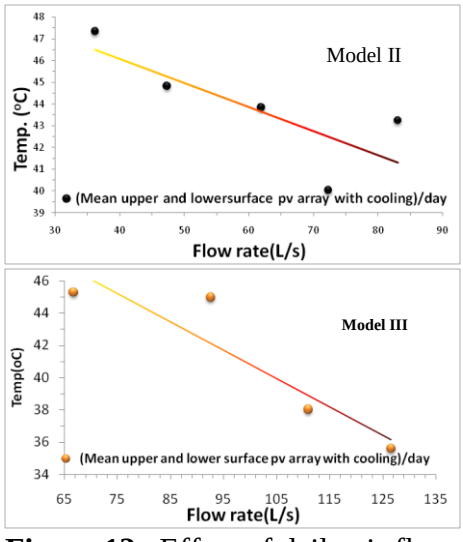

Figure 12. Effect of daily air flow rate on PV panel temp. for models II & III

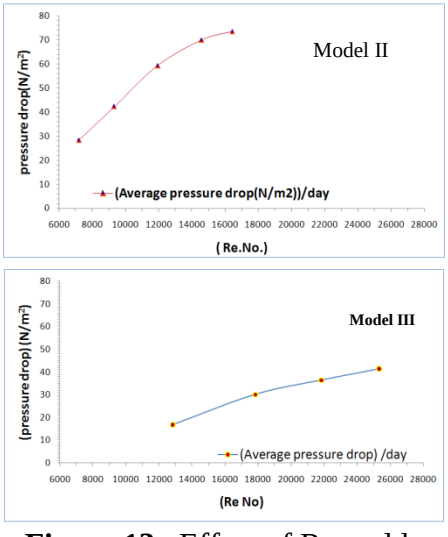

Figure 13. Effect of Reynolds number on pressure drop for models II & III

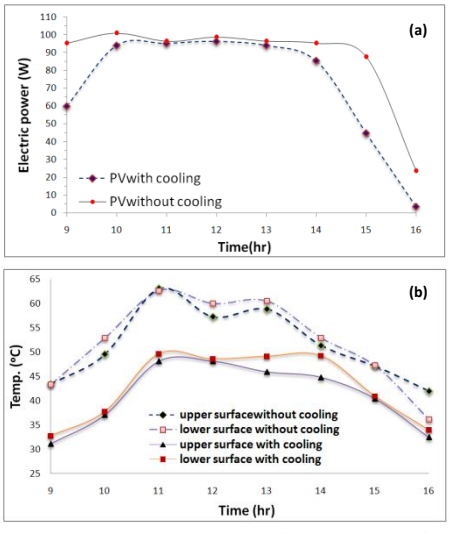

Figure 14. (a) Hourly electrical power produced by models I& II on (29/3/2011) (b) Hourly temperature distribution of the upper and lower PV panel on (29/3/2011) for models I&II

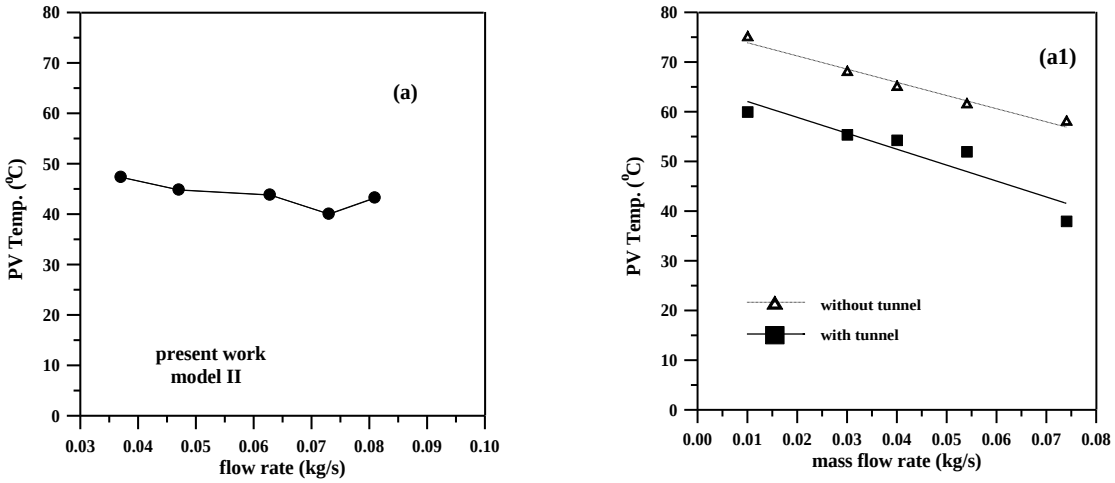

Effect of air mass flow rate on temperature of PV module for collector model II,
(a) present results, (a1) results of **(Jin et al. 2010)**

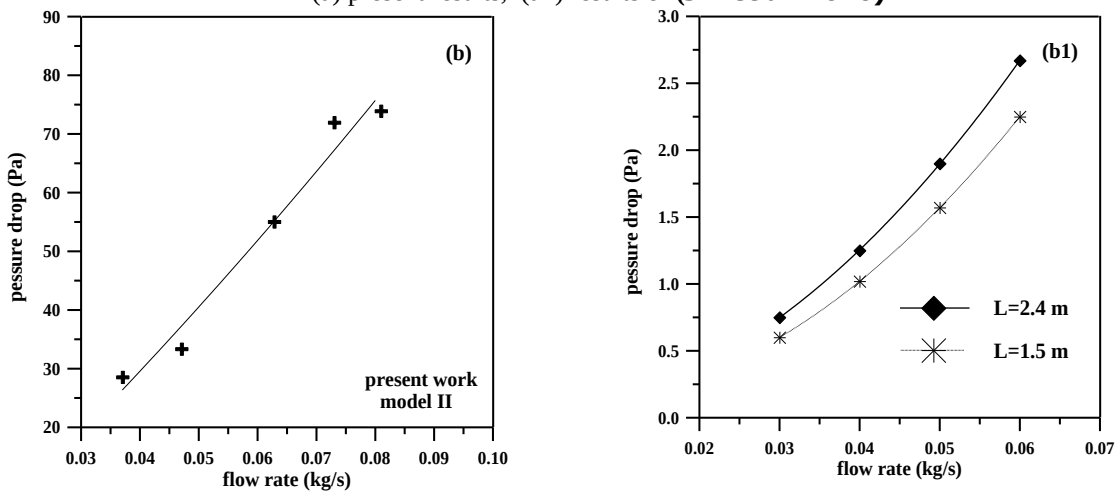

Effect of air mass flow rate on pressure drop for collector model II,
(b) present results, (b1) results of **(Baa 2008)**

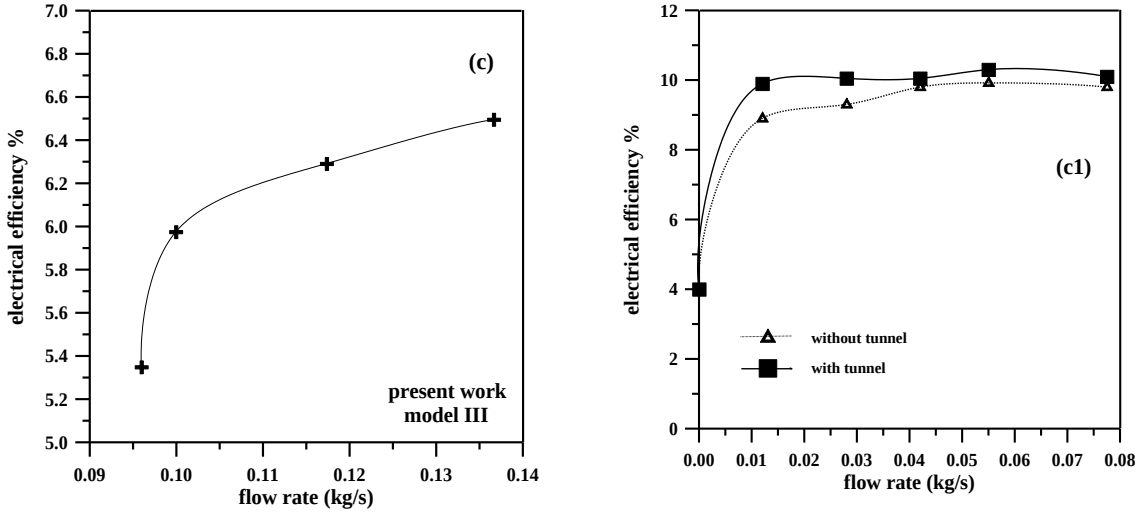

Effect of mass flow rate on electrical efficiency PV module for collector model III,
(c) present results, (c1) results of **(Jin et al. 2010)**

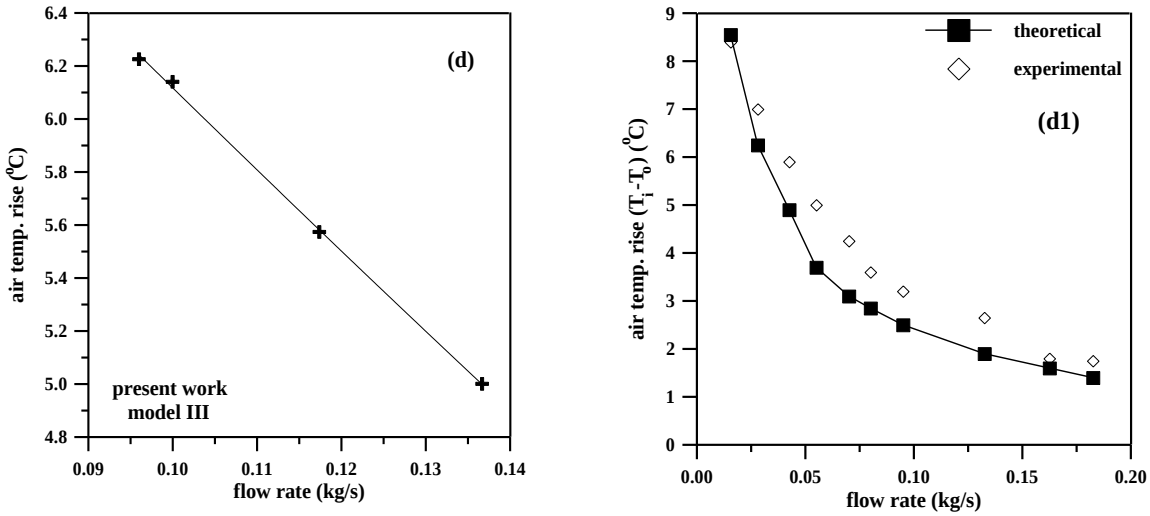

Effect of mass flow rate on air temperature rise for collector model III,
(d) present results, (d1) results of **(Othman et al.2007)**

Figure 15. Comparison of the present results with previously published results.

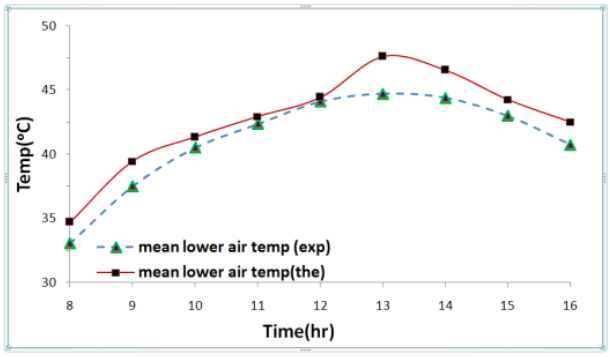

Figure 16. Comparison between theoretical and experimental values of hourly air temperature on (2/7/2011) for model IV

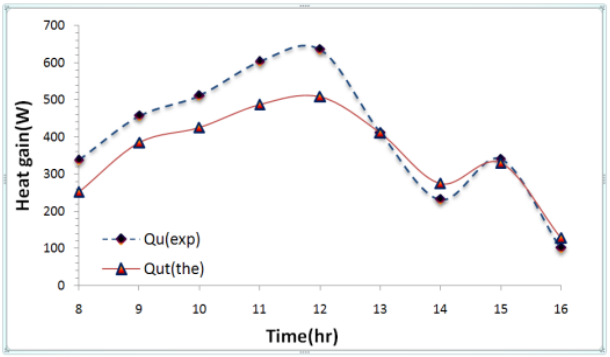

Figure 17. hourly comparison between theoretical and experimental values of hourly heat gain on (2/7/2011) for model IV

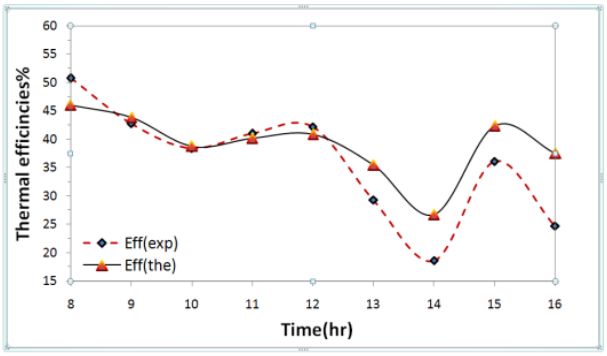

Figure 18. Comparison between theoretical and experimental values of hourly thermal efficiency on (2/7/2011) for model IV